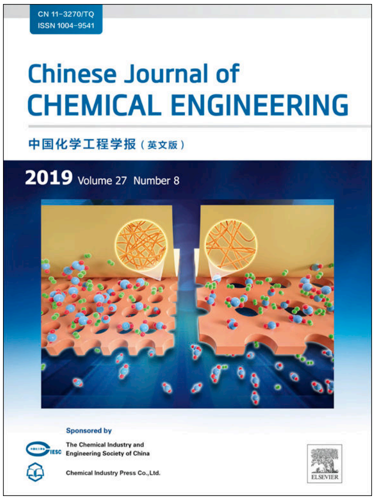

Full Length Article

The dynamic evolution of aggregated Li dendrites in lithium metal batteries

Xin Shen, Rui Zhang, Shuhao Wang, Xiang Cheng, Chuan Zhao, Elena Kuzmina, Elena Karaseva, Vladimir Kolosnitsyn, Qiang Zhang

PII: S1004-9541(21)00239-1
DOI: https://doi.org/10.1016/j.cjche.2021.05.008
Reference: CJCHE 2264

To appear in: *Chinese Journal of Chemical Engineering*

Received Date: 27 January 2021
Revised Date: 16 April 2021
Accepted Date: 8 May 2021

Please cite this article as: X. Shen, R. Zhang, S. Wang, X. Cheng, C. Zhao, E. Kuzmina, E. Karaseva, V. Kolosnitsyn, Q. Zhang, The dynamic evolution of aggregated Li dendrites in lithium metal batteries, *Chinese Journal of Chemical Engineering* (2021), doi: https://doi.org/10.1016/j.cjche.2021.05.008

Invited Manuscript for Advanced Chemical Engineering of Energy Materials in Chinese Journal of Chemical Engineering

The dynamic evolution of aggregated Li dendrites in lithium metal batteries

***Xin Shen*[1], *Rui Zhang*[2], *Shuhao Wang*[3], *Xiang Cheng*[1], *Chuan Zhao*[3]**, *Elena Kuzmina*[4], *Elena Karaseva*[4], *Vladimir Kolosnitsyn*[4], ***Qiang Zhang*[1,*]**

[1]**Beijing Key Laboratory of Green Chemical Reaction Engineering and Technology, Department of Chemical Engineering, Tsinghua University, Beijing 100084, China.**

[2]**Advanced Research Institute of Multidisciplinary Science, Beijing Institute of Technology, Beijing 100081, China.**

[3]**School of Chemistry, The University of New South Wales, Sydney, NSW 2052, Australia.**

[4] Laboratory of Electrochemistry, Ufa Institute of Chemistry—Subdivision of the Ufa Federal Research, Centre of the Russian Academy of Sciences, 69, prospect Oktyabrya, Ufa 450054, Russia.

[*]**Corresponding author**. E-mail: zhang-qiang@mails.tsinghua.edu.cn (Q. Zhang)

Article

The dynamic evolution of aggregated lithium dendrites in

lithium metal batteries

Xin Shen[1], Rui Zhang[2], Shuhao Wang[3], Xiang Chen[1], Chuan Zhao[3], Elena Kuzmina[4], Elena Karaseva[4], Vladimir Kolosnitsyn[4], Qiang Zhang[1,]*

[1]Beijing Key Laboratory of Green Chemical Reaction Engineering and Technology, Department of Chemical Engineering, Tsinghua University, Beijing 100084, China.

[2]Advanced Research Institute of Multidisciplinary Science, Beijing Institute of Technology, Beijing 100081, China.

[3]School of Chemistry, The University of New South Wales, Sydney, NSW 2052, Australia.

[4] Laboratory of Electrochemistry, Ufa Institute of Chemistry—Subdivision of the Ufa Federal Research, Centre of the Russian Academy of Sciences, 69, prospect Oktyabrya, Ufa 450054, Russia.

[*]**Corresponding author**. E-mail: zhang-qiang@mails.tsinghua.edu.cn (Q. Zhang)

Abstract

Lithium (Li) metal anodes promise an ultrahigh theoretical energy density and low redox potential, thus being the critical energy material for next-generation batteries. Unfortunately, the formation of Li dendrites in Li metal anodes remarkably hinders the practical applications of Li metal anodes. Herein, the dynamic evolution of discrete Li dendrites and aggregated Li dendrites with increasing current densities is visualized by *in-situ* optical microscopy in conjunction with *ex-situ* scanning electron microscopy. As revealed by the phase field simulations, the formation of aggregated Li dendrites under high current density is attributed to the locally concentrated electric field rather than the depletion of Li ions. More specifically, the locally concentrated electric field stems from the spatial inhomogeneity on the Li metal surface and will be further enhanced with increasing the current densities. Adjusting the above two factors with the help of the constructed phase field model is able to regulate the electrodeposited morphology from aggregated Li dendrites to discrete Li dendrites, and ultimately columnar Li morphology. The methodology and mechanistic understanding established herein give a significant step toward the practical applications of Li metal anodes.

Keywords: Electrochemistry, Li dendrites, rechargeable Li batteries, *in-situ* optical microscopy, phase field model, electrochemical engineering

1. Introduction

Lithium (Li) metal has attracted widespread interests as an ideal anode for next-generation batteries because of its high theoretical capacity (3860 $mAh \cdot g^{-1}$) and low redox potential (−3.04 V *vs.* the stand hydrogen electrode) [1-3]. The batteries based on Li metal anodes can deliver a striking improvement in practical energy density (> 400 $Wh \cdot kg^{-1}$), especially Li–S and Li–O_2 systems [4-5]. Unfortunately, the practical application of Li metal anodes is rather troublesome due to the uncontrolled formation of Li dendrites, which induces a poor cycle life, low Coulombic efficiency, and even safety concern [6-7]. Therefore, a deep understanding of the dynamic evolution of Li dendrites and valid regulation methods are strongly requested [8-9].

Generally, Li dendrites refer to the unordered non-planar electrodeposits [10]. In 1979, Chianelli *et al.* described the observation of Li dendrites for the first time [11]. Since then, tremendous studies have been devoted to investigating the morphology of Li dendrites through *in/ex-situ* microscopy [12-17]. In spite of ubiquitous metal dendrites in the electrodeposition, the high reactivity of Li metal, which brings about solid electrolyte interphase (SEI) [18-20], endows more specificity and diversity to Li dendrites. Up to now, there is no consensus of the description on Li dendrites. Li dendrites can be classified into two types: An individual Li dendrite, which can be identified as needle-like [21-22], whisker-like [23], and filament-like structures [24]; An aggregated Li dendrite, which is likely to be described as moss-like [25], bush-like [26], and tree-like Li dendrite structures [27]. Both the thermodynamic and kinetic factors, such as surface diffusion [28-29], ion/electron transfer [30-33], stress extrusion

[34], and temperature [35-36], have been explored to interpret various final morphologies. In view of dynamic evolution, various growth modes of Li dendrites, including tip growth, root growth, and "bread expansion" [26], are proposed. However, a comprehensive understanding of the relationship between the individual and aggregated Li dendrites is lacking: 1) why individual dendrites cluster into aggregated Li dendrites; 2) if individual dendrites can be arranged in an orderly manner with consistent size, direction, and growth rate, which likes the columnar deposited morphology.

In this contribution, multiscale imaging techniques (e.g. *in-situ* optical microscopy, *ex-situ* scanning electron microscopy (SEM)) were employed to capture the evolution of Li electrodeposition, especially the aggregated Li dendrites. Specifically, the growth of aggregated Li dendrites inhibits the growth of surrounding discrete Li dendrites. Further mechanistic understanding through correlation with a phase field model is provided. It is revealed that the locally concentrated electric field stemming from the spatial heterogeneity along the Li metal surface is exacerbated by increasing the applied current density, which results the formation of aggregated Li dendrites.

2. Materials and Methods

2.1. Materials

Li foils of 50-μm thickness were purchased from China Energy Lithium Co., Ltd. Copper (Cu) foils were purchased from Shenzhen Kejing Star Technology Co., Ltd. The electrolyte purchased from Beijing Institute of Chemical Reagents is composed of lithium hexafluorophosphate ($LiPF_6$, 1.0 mol·L^{-1}) dissolved in ethylene carbonate (EC)/diethyl carbonate (DEC) (1:1 by volume). Celgard 2400 was employed as the separator. All materials were reserved in an Ar-filled glove box with oxygen and water contents below 0.1 ppm.

2.2. ***In-situ* optical microscopy**

The *in-situ* optical Li | Li symmetric cell with a quartz window was fabricated and assembled as Fig. 1. Specially, lithium foils were rolled on the Cu foils in advance and were employed as the electrodes. The distance between the anode and cathode is about 1.0 mm. All operations were carried out in the glove box. Solartron 1470E electrochemical workstation was employed to provide the constant current and record the voltage–time profile. The optical microscope (Nikon SMZ25) with a camera (Nikon DS-Fi3 Microscope Camera) was used to catch the morphological evolution of Li surface during electroplating. The videos were recorded at 30 frame/s with NIS-Elements D software.

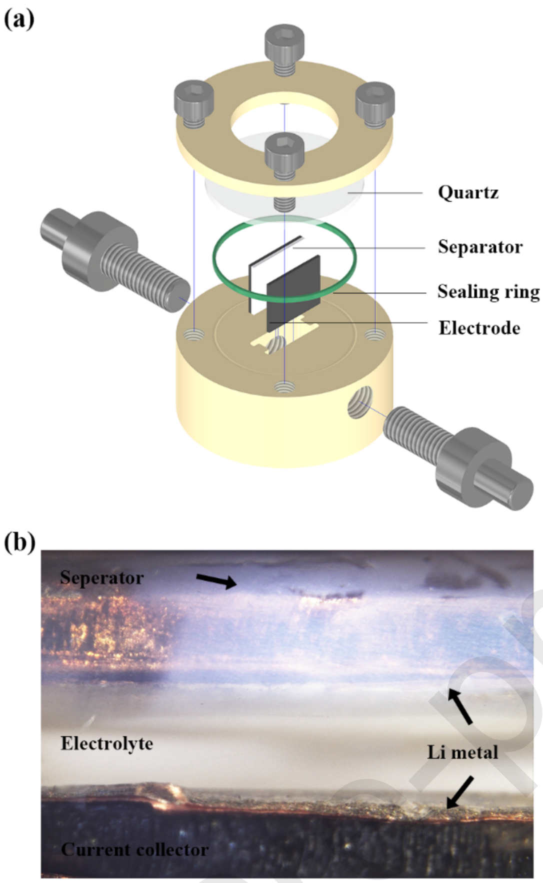

Fig. 1. The *in-situ* optical cell. (a) Schematic diagram. (b) The optical image of the cell section.

2.3. *Ex-situ* scanning electron microscopy

Scanning electron microscopy (SEM) images were acquired from JSM 7401F, JEOL Ltd., Japan. The Li metal anodes obtained from *in-situ* optical Li | Li symmetric cell were rinsed with the pure solvent (DEC) and then dried thoroughly in the glove box prior to characterization. Samples were kept under argon conditions utilizing a home-made transfer vessel.

2.4. Phase field simulation

The phase field simulation is based upon our previous reported model [37]. An order parameter ξ is employed to differentiate the phases, defined as ξ = 1 and 0 for the Li metal and electrolyte, respectively.

The morphology evolution under electroplating ($\mathrm{Li}^+ + \mathrm{e}^- \rightarrow \mathrm{Li}$) is expressed by a modified Butler–Volmer equation,

$$\frac{\partial \xi}{\partial t} = -L_\sigma\left(g'(\xi) + f'_{\mathrm{grad}}(\xi) + f'_{\mathrm{noise}}(\xi)\right) - L_\eta h'(\xi)\left(\mathrm{e}^{\frac{(1-\alpha)F\eta}{RT}} - \frac{c_{\mathrm{Li}^+}}{c_0}\mathrm{e}^{\frac{-\alpha F\eta}{RT}}\right) \tag{1}$$

where L_σ is the interfacial mobility, L_η the reaction constant, α the charge-transfer coefficient, c_0 the initial concentration of electrolyte, η the overpotential, R the molar gas constant, T the temperature, F the Faraday constant. The overpotential η can be calculated by $\Delta\phi - E_{eq}$, where ϕ is the electrostatic potential, E_{eq} the equilibrium potential. $g(\xi) = W\xi^2(1-\xi)^2$ is an arbitrary double well function, where $W/16$ represents the barrier height. $f_{\mathrm{grad}}(\xi) = \frac{1}{2}\kappa_0[1 + \delta\cos(\omega\theta)]\nabla^2\xi$ is the gradient energy density, where κ_0 is the gradient energy coefficient, δ the strength of anisotropy, ω the mode of the anisotropy, and θ the angle between the normal vector of the interface and the reference axis. $f_{\mathrm{noise}}(\xi) = h'(\xi)\psi$ is a noise function, represents the spatial heterogeneity. $h(\xi) = \xi^3(6\xi^2 - 15\xi + 10)$ is an interpolating function. ψ is a random function.

The evolution of Li ion concentration is described by the Nernst–Planck equation,

$$\frac{\partial c_{\mathrm{Li}^+}}{\partial t} = \nabla \cdot \left(D_{\mathrm{Li}^+}\nabla c_{\mathrm{Li}^+} + D_{\mathrm{Li}^+}c_{\mathrm{Li}^+}\frac{F}{RT}\nabla\phi\right) - c_{\mathrm{Li}}\frac{\partial \xi}{\partial t} \tag{2}$$

where D_{Li^+} is the diffusion coefficient of Li^+, c_{Li} the initial concentration of Li atoms.

The electrostatic potential can be expressed by

$$\nabla \cdot (\sigma_{\mathrm{eff}}\nabla\phi) = Fc_{\mathrm{Li}}\frac{\partial \xi}{\partial t} \tag{3}$$

where $\sigma_{\mathrm{eff}} = h(\xi)\sigma_{\mathrm{Li}} + (1 - h(\xi))\sigma_{\mathrm{e}}$ is the effective electric conductivity. σ_{Li} and σ_{e} represent the electric conductivity of electrode and electrolyte, respectively.

Above equations were solved by COMSOL Multiphysics 5.5. A 2D domain (100 × 100 μm) is adopted. The initial morphology of Li nuclei is representing by semi-spheres with a radius of 0.5 μm and an interval of 4.0 μm. Dirichlet boundary conditions are applied on the top and bottom boundary for the Li ion concentration and electrostatic potential. The Li ion concentration on the top boundary is fixed to 1.0 M, representing the bulk solution; The electrostatic potential on the bottom boundary is fixed to 0 V as grounding. Global equations are employed to satisfy that the internal current density equals to applied current density. All model parameters are listed in Table 1.

Table 1. Model parameters employed in the phase field simulations.

Parameter	Value	Description	Reference
L_σ/ $\mathrm{m^3 \cdot J^{-1} \cdot s^{-1}}$	1×10^{-9}	Interfacial mobility	[38-39]*
L_η/ $\mathrm{s^{-1}}$	0.4	Reaction constant	[38-39]*
κ_0/ $\mathrm{J \cdot m^{-1}}$	2×10^{-6}	Gradient energy coefficient	[38-39]*
δ	0.03	The strength of anisotropy	[39]
ω	4	A mode number of anisotropy	[39]
W/ $\mathrm{J \cdot m^{-3}}$	1×10^{8}	Barrier height	[38-39]*
$D_{\mathrm{Li^+}}$/ $\mathrm{m^2 \cdot s^{-1}}$	3×10^{-10}	Diffusion coefficient of $\mathrm{Li^+}$ in electrolyte	[40]
c_0/ $\mathrm{mol \cdot m^{-3}}$	1000	Initial concentration of electrolyte	-
c_{Li}/ $\mathrm{mol \cdot m^{-3}}$	7.69×10^{4}	Initial concentration of electrode	[41]
σ_{Li}/ $\mathrm{S \cdot m^{-1}}$	1×10^{7}	Electrical conductivity of electrode	[41]
σ_{e}/ $\mathrm{S \cdot m^{-1}}$	1.0	Electrical conductivity of electrolyte	[40]
α	0.5	Charge transfer coefficients	[39]
T/ K	298.15	Temperature	-

Note: superscript * represents the value estimated based on the references.

3. Results and Discussions

To track the dynamic evolution of Li dendrites, *in-situ* optical observation was conducted in a special Li | Li symmetric cell (Fig. 1). Compared to postmortem analyses, *in-situ* optical microscopy can offer an *in-situ* and true-color observation. Herein a routine electrolyte of 1.0 mol•L^{-1} LiPF$_6$ in EC/DEC was used. The electrodeposition was propelled by a constant current density of 1.0 mA·cm^{-2} and the total plating time was set as 3.0 h.

Synchronized morphology and voltage profile of electrodeposition are shown in Fig. 2 and Video S1 (Supporting Information). The open circuit voltage of the Li | Li symmetric cell is around 0 V. Once the constant current is applied, the voltage starts to drop until a minimum, whereafter asymptotically reaches a relatively stable value (Fig. 2a). Although a thick electrolyte layer in the optical cell brings a large ohmic resistance, the voltage trace is consistent with that of a coin cell. Such voltage profile is a typical response signal during the Li electrodeposition, which corresponds to the formation of SEI, Li nucleation, and the growth of Li dendrites (Fig. 2b–g). Dasgupta and co-workers have carried out immense study to untangling the relationship between voltage variations and morphology evolution [42-43]. Herein we focus on the electrodeposited morphology. Theoretically, the thickness of the planar electrodeposited Li (h) is defined by

$$h = \frac{i_{\mathrm{applied}} t M_{\mathrm{Li}}}{F \rho_{\mathrm{Li}}} \qquad (4)$$

where i_{applied} is the applied current density, t the plating time, M_{Li} the atomic weight of

Li, ρ_{Li} the mass density of Li metal. In this case, the thickness of the planar electrodeposited Li is about 14.5 μm, which is almost invisible in the optical microscope. However, an aggregated Li dendrite with a height of *ca.* 300 μm appeared at a plating capacity of 0.5 mAh·cm^{-2} (Fig. 2d). As the electrodeposition advances, it continues to expand without a preferred grow site, just like a bread fermentation. It is consistent with the description of Li bush growth that reported by Steiger *et al* [26]. The ultimate thickness of this aggregated dendrite reaches 800 μm, much larger than the theoretical deposition thickness. It can be supposed that the aggregated dendrite becomes a hot spot and attracts all deposited Li ions. Apparently, the aggregated dendrite is undesirable, which not only brings huge volume expansion, but also increases the formation risk of dead Li in the stripping process.

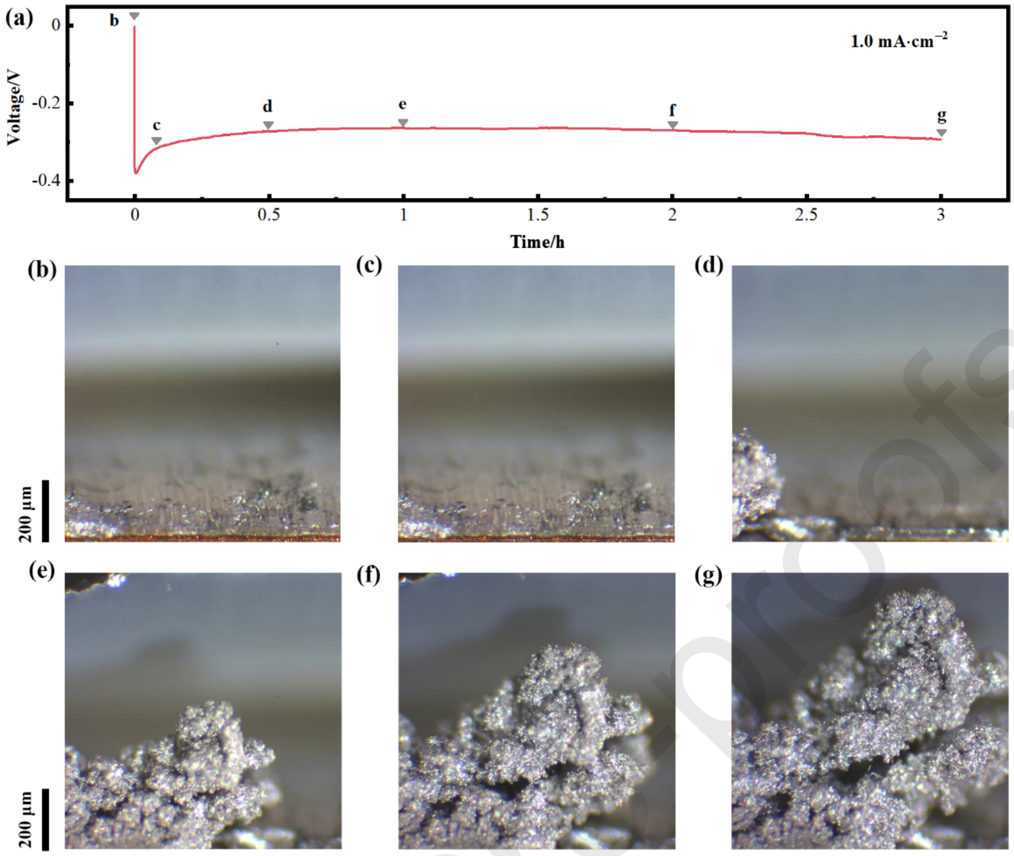

Fig. 2. Observation of Li electrodeposition in the *in-situ* Li | Li symmetric cell cycled at 1.0 mA·cm^{-2}. (a) Voltage responses with respect to plating time. (b–g) *In-situ* optical snapshots of Li dendrites growth during electroplating.

Further observations at various current densities were carried out (Fig. 3 and Video S2, Supporting Information). When increasing the current density to 3.0 mA·cm^{-2}, an aggregated Li dendrite was observed (Fig. 3a–d). Under a same plating capacity, the Li dendrite formed at a higher current density of 3.0 mA·cm^{-2} (Fig. 3b) exhibits a similar height (about 800 μm) but more fractal shape compared to that formed at 1.0 mA·cm^{-2} (Fig. 2g). Limited by the resolution of optical microscopy, the fine structure inside the aggregated Li dendrite is invisible. In this regard, postmortem characterization of SEM was carried out after optical observation, achieving a resolution complement [44]. Fig. 3c and d demonstrates that the aggregated Li dendrites in optical images is not integrated and solid, but consists of Li whiskers. These whiskers are inconsistent in size and are entangled with each other, making it impossible to distinguish the onsets and ends. In contrast, no obvious aggregated Li dendrite formation at 0.5 mA·cm^{-2} before a plating capacity of 2.7 mAh·cm^{-2} (Fig. 3e–g, Video S2, Supporting Information). Only a tiny bump emerged after a plating capacity of 3.0 mAh·cm^{-2} (marked in Fig. 3f). Moreover. it can be found that the surface roughness of Li metal has changed, resulting in the weakness of reflected light on the Li metal surface. There are massive needle-like Li dendrites (a diameter of about 2.0 μm and a height of about 10.0 μm) on the Li metal surface (Fig. 3g, h). It is a relatively uniform and compact electrodeposition.

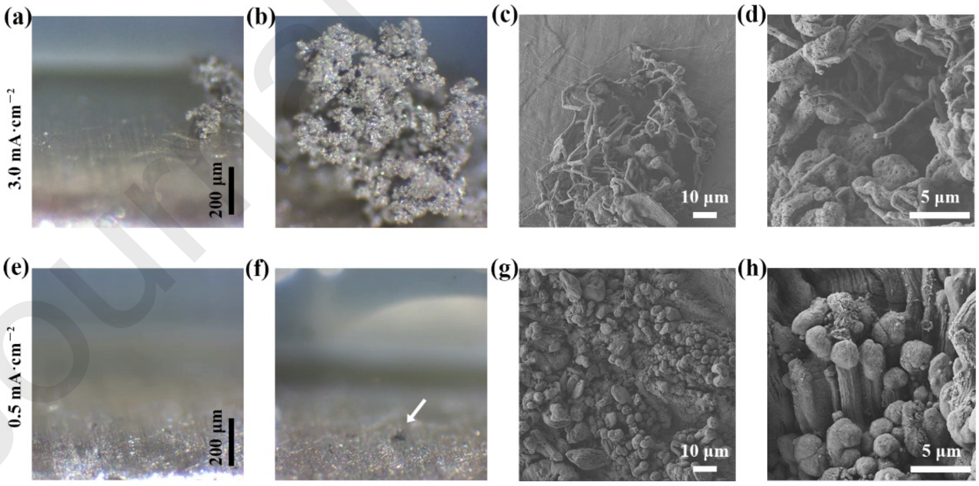

Fig. 3. Li dendrites growth at 3.0 mA·cm^{-2} (a–d) and 0.5 mA·cm^{-2} (e–f). *In-situ* optical snapshots with a plating capacity of 0.08 mAh·cm^{-2} (a, e) and 3.0 mAh·cm^{-2} (b, f), respectively. (c, d, g, h) *ex-situ* SEM images after optical observations.

In summary, there are two different phenomena in the above experiments: 1) all Li ions are deposited in one site under a large current density, resulting in a huge aggregated dendrite; 2) the nucleation sites grow into whisker-like Li together under a small current density. Previous work has indicated that the number density of nuclei raises with the increasing of current density [45]. Obviously, the surface density distribution of Li density in the growth process is opposite to the nucleation process. Therefore, the formation of aggregated Li dendrites is determined by the latter growth process rather than the nucleation process. While the current density exceeding the limiting current density, the occurrence of dendritic morphology has been well understood by Sand's time model and Chazalviel model [46-47]. Therefore we estimated the limiting current density by

$$J_{\lim} = \frac{FDc_0}{(1 - t_+)L/2} \tag{5}$$

where F denotes Faraday's constant, $D = 3\times10^{-6}\ \mathrm{cm^2\cdot s^{-1}}$ the diffusion coefficient, c_0 the bulk concentration, $t_+ = 0.38$ the cation transference number, $L = 1.0$ mm the distance between the two electrodes [40]. The calculated value of limiting current density is 9.4 $\mathrm{mA\cdot cm^{-2}}$. It means that the electrodeposition observed in this work are under mixed diffusion and kinetic control, where the depletion of interfacial Li ion is unable. Therefore, it is difficult to interpret the phenomena with the classic models.

An important disturbance that the Sand's time model transplanted from Cu electrodeposition does not consider is the heterogeneity caused by the SEI and other impurities of the Li surface. In this regard, phase field simulations were performed for explaining above phenomena. Comparing with our previous model [37], spatial heterogeneities stemming from SEI or other factors are involved in this work, represented by a noise function (See section 2.4. Phase field simulation). Moreover, the variation of Li nuclei under different current densities, including space density and size, are ignored. We assume that the initial nuclei exist in the form of semi-spheres with a fixed radius of 0.5 μm and a fixed interval of 4.0 μm.

The simulated results and quantitative data are presented in Fig. 5 and Fig. 6. Fig. 5a and c display the simulated morphology of electrodeposited Li as well as the distribution of Li ion concentration at a plating capacity of 0.1, 1.0, 2.0, and 3.0 mAh·cm^{-2}, respectively, in which $\xi = 1$ and 0 represent the Li metal and electrolyte, respectively. The dynamic evolution of morphology is illustrated in Video S3 (Supporting Information). The simulated morphology is consistent with the experiment results. There are aggregated Li dendrites on the Li meta anode surface at a current density of 3.0 mA·cm^{-2}. This inhibits the growth of surrounding discrete Li dendrites. In the case of 0.5 mA·cm^{-2}, discrete Li nuclei grow together at first, presenting a columnar-like morphology (before 1.0 mAh·cm^{-2}). Then their growth rate diverges, resulting in a variation of diameter and height (2.0 and 3.0 mAh·cm^{-2}). These discrete dendrites are able to evolve into columnar Li morphology with an efficient regulation. The ratio of current deposit surface area S_{current} to the initial deposit surface area S_{initial} affords an objective indicator for the morphology evolution. It is noted that $S_{\text{current}}/S_{\text{initial}}$ under ideal planar electrodeposition keeps in a value of 1.0. As shown in Fig. 6a, $S_{\text{current}}/S_{\text{initial}}$ under 3.0 mA·cm^{-2} increases almost linearly to 7.01, 13.10, and 18.47 at

1.0, 2.0, and 3.0 mAh·cm^{-2}, respectively. In contrast, $S_{\mathrm{current}}/S_{\mathrm{initial}}$ under 0.5 mA·cm^{-2} sluggishly increases to 5.13, 7.45, and 8.89 at 1.0, 2.0, and 3.0 mAh·cm^{-2}, respectively. This indicates that the larger current density, the higher degree of dendrite fractal. The rapidly rise of exposed surface area renders a large amount of SEI, thereby affecting the performance of the batteries [48].

Furthermore, the minimum value of Li ion concentration near the Li surface at 0.5 mA·cm^{-2} and 3.0 mAh·cm^{-2} is 0.54 M (the last column of Fig. 5c). Although this value decreases to 0.36 M with the increase of current density (3.0 mA·cm^{-2}), it still does not reach 0 (the last column of Fig. 5a). It demonstrates that the Li ion near the Li surface is never depleted, which agrees with our previous discussion about the limiting current density. Then what caused the transition of aggregated Li dendrites from discrete Li dendrites?

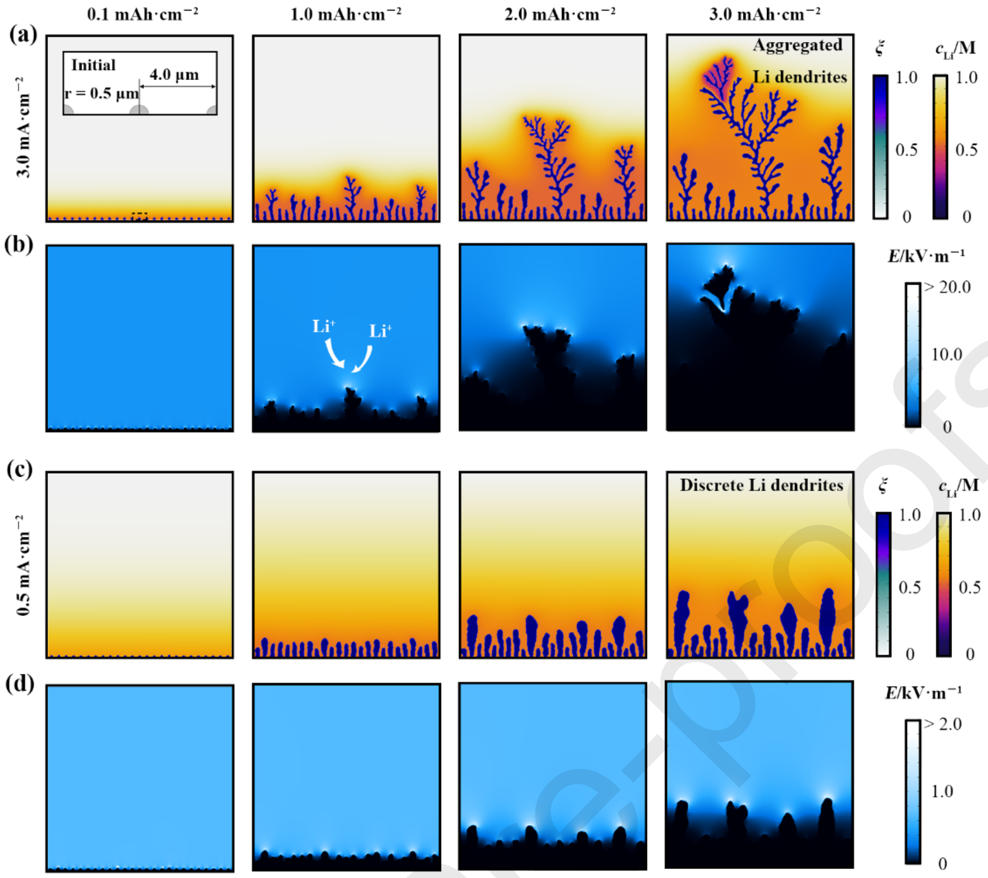

Fig. 4. The simulated results of Li dendrites. The simulated (a, c) dendritic morphology evolution, Li ion concentration, and (b, d) corresponding electric field intensity during Li electroplating at 3.0 mA·cm^{-2} (a, b) and 0.5 mA·cm^{-2} (c, d), respectively. Inset: A schematic of the initial Li nuclei.

Corresponding electric field distribution gives an intuitive explanation, which is exhibited in Fig. 5b and d. At first, the electric field on the surface of Li metal is relatively uniform (0.1 mAh·cm^{-2}), where small fluctuation is induced by the space heterogeneity. With the electroplating advances, locally electric field around some tips of Li dendrites is quickly enhanced. Compared to the case of a small current density, the tip with locally max electric field forms a strong shielding effect, which intensely attracts the Li ions and finally forms aggregated Li dendrites. The quantitative analyses of the electric field intensity around the tips of Li dendrites with the variation in applied current density and plating capacity are shown in Fig. 6b. With the increasing of the applied current density from 0.5 to 3.0 mA·cm^{-2}, about six fold the average electric field intensity at a plating capacity of 0.1 mAh·cm^{-2} is enhanced from about 1.0 to 6.0 kV·m^{-1}. After further electrodeposition (1.0 mAh·cm^{-2}), the fluctuation of electric field strength is amplified. For 0.5 mA·cm^{-2}, the fluctuation is within 2 kV·m^{-1}, whereas it reaches 20 kV·m^{-1} at 3.0 mA·cm^{-2}.

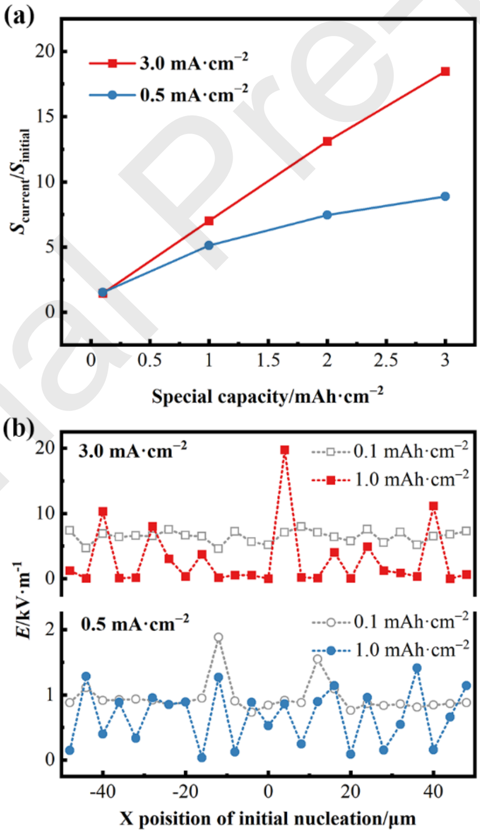

Fig.5. Quantitative data from phase field simulations. (a) The growth rate of surface area with respect to plating capacity. (b) The electric field intensity around dendrite tips with respect to the position of initial nucleation.

According to above results and discussion, the aggregation of individual Li dendrites stems from the spatial inhomogeneity, which is further amplified by the current density, resulting in a locally concentrated electric field. Even if the limiting current density is unreached, such locally concentrated electric field is enough to form a hot spot, attracting subsequent deposited Li ions, suppressing the growth of surrounding discrete Li dendrites, and finally developing into aggregated Li dendrites. Therefore, it is insufficient to regulate Li dendrites according to the limiting current density and Sand's time. Reducing the actual current density of Li metal anodes helps to delay the formation of aggregated Li dendrites, but the most fundamental thing should be to regular the spatial heterogeneity of the Li surface. This is especially important as Li metal batteries evolve into harsh conditions, *e.g.*, electrode with large area (from coin cells to pouch cells), high current density, lean electrolyte, and low negative/positive capacity ratio[49]. In this respect, a Li host or an ion re-distribution layer might help flatten the spatial heterogeneity.

4. Conclusions

Various electrodeposited morphologies in the Li metal anodes were visualized by means of *in-situ* optical microscopy and *ex-situ* SEM, especially the transition from discrete Li dendrites to aggregated Li dendrites with increasing current densities. Combining with the phase field simulations, it is quantitatively revealed that the dynamic evolution of aggregated Li dendrites is induced by the locally concentrated electric field rather than the depletion of Li ions. Specifically, the locally concentrated electric field originates from the spatial inhomogeneity on the Li metal surface and can be further enhanced by the high operating current density. Adjusting these two factors—with the assistance of the constructed phase field model—is able to regulate the electrodeposited morphology from aggregated Li dendrites to discrete Li dendrites, and finally realize ideal columnar Li morphology. Besides, it is appealed that more accessible and paralleled parameters, especially the kinetic parameters of electrolytes and SEI should be afforded in the future experiment research. The deep and fundamental understanding of various Li electrodeposition morphology established herein sheds light to the regulation of Li dendrites.

Acknowledgements

This work was supported by the National Natural Science Foundation of China (22061132002, U1801257, and 21825501), the National Key Research and Development Program (2016YFA0200102 and 2016YFA0202500), Beijing Municipal Natural Science Foundation (Z20J00043), and the Tsinghua University Initiative Scientific Research Program.

Supplementary Materials

The Supporting Information is available online.

Video S1: Synchronized morphology and voltage profile cycled at 1.0 mA·cm^{-2}

Video S2: Morphology evolution at the current of 3.0 mA·cm^{-2} and 0.5 mA·cm^{-2}

Video S3: Simulated morphology by phase field model at the current of 3.0 mA·cm^{-2} and 0.5 mA·cm^{-2}

References

[1] X. Shen, X.Q. Zhang, F. Ding, J.Q. Huang, R. Xu, X. Chen, C. Yan, F.Y. Su, C.M. Chen, X.J. Liu, Q. Zhang, Advanced electrode materials in lithium batteries: Retrospect and prospect. *Energy Mater. Adv.* 2021 (2021) 1205324.

[2] F. Wu, J. Maier, Y. Yu, Guidelines and trends for next-generation rechargeable lithium and lithium-ion batteries. *Chem. Soc. Rev.* 49 (2020) 1569–1614.

[3] R.H. Wang, W.S. Cui, F.L. Chu, F.X. Wu, Lithium metal anodes: Present and future. *J. Energy Chem.* 48 (2020) 145–159.

[4] Y.X. Yao, X.Q. Zhang, B.Q. Li, C. Yan, P.Y. Chen, J.Q. Huang, Q. Zhang, A compact inorganic layer for robust anode protection in lithium-sulfur batteries. *InfoMat* 2 (2020) 379–388.

[5] J. Zheng, M.S. Kim, Z. Tu, S. Choudhury, T. Tang, L.A. Archer, Regulating electrodeposition morphology of lithium: towards commercially relevant secondary Li metal batteries. *Chem. Soc. Rev.* 49 (2020) 2701–2750.

[6] K.N. Wood, M. Noked, N.P. Dasgupta, Lithium metal anodes: Toward an improved understanding of coupled morphological, electrochemical, and mechanical behavior. *ACS Energy Lett.* 2 (2017) 664–672.

[7] H. Liu, X.B. Cheng, Z.H. Jin, R. Zhang, G.X. Wang, L.Q. Chen, Q.B. Liu, J.Q. Huang, Q. Zhang, Recent advances in understanding dendrite growth on alkali metal

anodes. *EnergyChem* 1 (2019) 100003.

[8] J.F. Ding, R. Xu, C. Yan, Y. Xiao, Y.R. Liang, H. Yuan, J.Q. Huang, Integrated lithium metal anode protected by composite solid electrolyte film enables stable quasi-solid-state lithium metal batteries. *Chin. Chem. Lett.* 31 (2020) 2339–2342.

[9] J. Liu, H. Yuan, X. Tao, Y. Liang, S.J. Yang, J.Q. Huang, T.Q. Yuan, M.M. Titirici, Q. Zhang, Recent progress on biomass-derived ecomaterials toward advanced rechargeable lithium batteries. *EcoMat* 2 (2020) e12019.

[10] J. Xiao, How lithium dendrites form in liquid batteries. *Science* 366 (2019) 426–427.

[11] R.R. Chianelli, J.C. Scanlon, B.M.L. Rao, In situ studies of electrode reactions: The mechanism of lithium intercalation in TiS_2. *J. Solid State Chem.* 29 (1979) 323–337.

[12] J.H. Um, S.H. Yu, Unraveling the mechanisms of lithium metal plating/stripping via in situ/operando analytical techniques. *Adv. Energy Mater.* (2020) 2003004.

[13] T. Foroozan, S. Sharifi-Asl, R. Shahbazian-Yassar, Mechanistic understanding of Li dendrites growth by in-situ/operando imaging techniques. *J. Power Sources* 461 (2020) 228135.

[14] X. Shen, R. Zhang, X.B. Cheng, C. Guan, J.Q. Huang, Q. Zhang, Recent progress on in-situ observation and growth mechanism of lithium metal dendrites. *Energy Storage Sci. Technol.* 6 (2017) 345–360.

[15] H. Liu, X.B. Cheng, R. Xu, X.Q. Zhang, C. Yan, J.Q. Huang, Q. Zhang, Plating/stripping behavior of actual lithium metal anode. *Adv. Energy Mater.* (2019)

1902254.

[16] H.L. Fan, C.H. Gao, H. Jiang, Q.Y. Dong, B. Hong, Y.Q. Lai, A systematical study on the electrodeposition process of metallic lithium. *J. Energy Chem.* 49 (2020) 59–70.

[17] Y. Ma, S. Li, B. Wei, Probing the dynamic evolution of lithium dendrites: a review of in situ/operando characterization for lithium metallic batteries. *Nanoscale* 11 (2019) 20429–20436.

[18] E. Peled, The electrochemical behavior of alkali and alkaline earth metals in nonaqueous battery systems-the solid electrolyte interphase model. *J. Electrochem. Soc.* 126 (1979) 2047–2051.

[19] Y.R. Liang, Y. Xiao, C. Yan, R. Xu, J.F. Ding, J. Liang, H.J. Peng, H. Yuan, J.Q. Huang, A bifunctional ethylene-vinyl acetate copolymer protective layer for dendrites-free lithium metal anodes. *J. Energy Chem.* 48 (2020) 203–207.

[20] Y. Shi, J. Wan, G.X. Liu, T.T. Zuo, Y.X. Song, B. Liu, Y.G. Guo, R. Wen, L.J. Wan, Interfacial Evolution of Lithium Dendrite and Its Solid Electrolyte Interphase Shell in Quasi-Solid-State Lithium Batteries. *Angew. Chem. Int. Ed.* 59 (2020) 18120–18125.

[21] M. Golozar, P. Hovington, A. Paolella, S. Bessette, M. Lagace, P. Bouchard, H. Demers, R. Gauvin, K. Zaghib, In situ scanning electron microscopy detection of carbide nature of dendrites in Li-polymer batteries. *Nano Lett.* 18 (2018) 7583–7589.

[22] I. Yoshimatsu, T. Hirai, J. Yamaki, Lithium electrode morphology during cycling in lithium cells. *J. Electrochem. Soc.* 135 (1988) 2422–2427.

[23] Y. He, X. Ren, Y. Xu, M.H. Engelhard, X. Li, J. Xiao, J. Liu, J.G. Zhang, W. Xu,

C. Wang, Origin of lithium whisker formation and growth under stress. *Nat. Nanotech.* 14 (2019) 1042–1047.

[24] J. Steiger, G. Richter, M. Wenk, D. Kramer, R. Monig, Comparison of the growth of lithium filaments and dendrites under different conditions. *Electrochem. Commun.* 50 (2015) 11–14.

[25] P. Bai, J. Li, F.R. Brushett, M.Z. Bazant, Transition of lithium growth mechanisms in liquid electrolytes. *Energy Environ. Sci.* 9 (2016) 3221–3229.

[26] J. Steiger, D. Kramer, R. Monig, Microscopic observations of the formation, growth and shrinkage of lithium moss during electrodeposition and dissolution. *Electrochim. Acta* 136 (2014) 529–536.

[27] C. Brissot, M. Rosso, J.N. Chazalviel, P. Baudry, S. Lascaud, In situ study of dendritic growth in lithium/PEO-salt/lithium cells. *Electrochim. Acta* 43 (1998) 1569–1574.

[28] B.S. Vishnugopi, F. Hao, A. Verma, P.P. Mukherjee, Surface diffusion manifestation in electrodeposition of metal anodes. *Phys. Chem. Chem. Phys.* 22 (2020) 11286–11295.

[29] M. Jäckle, K. Helmbrecht, M. Smits, D. Stottmeister, A. Groß, Self-diffusion barriers: possible descriptors for dendrite growth in batteries? *Energy Environ. Sci.* 11 (2018) 3400–3407.

[30] P. Bai, J.Z. Guo, M. Wang, A. Kushima, L. Su, J. Li, F.R. Brushett, M.Z. Bazant, Interactions between lithium growths and nanoporous ceramic separators. *Joule* 2 (2018) 2434–2449.

[31] X.Y. Xu, Y.Y. Liu, J.Y. Hwang, O.O. Kapitanova, Z.X. Song, Y.K. Sun, A. Matic, S.Z. Xiong, Role of Li-ion depletion on electrode surface: Underlying mechanism for electrodeposition behavior of lithium metal anode. *Adv. Energy Mater.* 10 (2020) 2002390.

[32] R. Zhang, X. Shen, J.F. Wang, Q. Zhang, Plating of Li ions in 3D structured lithium metal anodes. *CIESC J.* 71 (2020) 2688–2695.

[33] Z.K. Lin, Y.X. Qiao, W. Wang, H. Yuan, C. Fan, K.N. Sun, Morphology prediction of lithium plating by finite element modeling and simulations based on non-linear kinetics. *CIESC J.* 71 (2020) 4228–4237.

[34] A. Jana, S.I. Woo, K.S.N. Vikrant, R.E. García, Electrochemomechanics of lithium dendrite growth. *Energy Environ. Sci.* 12 (2019) 3595–3607.

[35] Y. Zhu, J. Xie, A. Pei, B. Liu, Y. Wu, D. Lin, J. Li, H. Wang, H. Chen, J. Xu, A. Yang, C.L. Wu, H. Wang, W. Chen, Y. Cui, Fast lithium growth and short circuit induced by localized-temperature hotspots in lithium batteries. *Nat. Commun.* 10 (2019) 2067.

[36] C.T. Love, O.A. Baturina, K.E. Swider-Lyons, Observation of lithium dendrites at ambient temperature and below. *ECS Electrochem. Lett.* 4 (2015) A24–A27

[37] R. Zhang, X. Shen, X.B. Cheng, Q. Zhang, The dendrite growth in 3D structured lithium metal anodes: Electron or ion transfer limitation? *Energy Storage Mater.* 23 (2019) 556–565.

[38] D.R. Ely, A. Jana, R.E. García, Phase field kinetics of lithium electrodeposits. *J. Power Sources* 272 (2014) 581–594.

[39] L. Chen, H.W. Zhang, L.Y. Liang, Z. Liu, Y. Qi, P. Lu, J. Chen, L.Q. Chen, Modulation of dendritic patterns during electrodeposition: A nonlinear phase-field model. *J. Power Sources* 300 (2015) 376–385.

[40] L.O. ValoÆn, J.N. Reimers, Transport properties of $LiPF_6$-based Li-ion battery electrolytes. *J. Electrochem. Soc.* 152 (2005) A882–A891.

[41] W.M. Haynes, D.R. Lide, T.J. Bruno, CRC handbook of chemistry and physics, 97th Edition, CRC Press, 2016.

[42] K.N. Wood, E. Kazyak, A.F. Chadwick, K.H. Chen, J.G. Zhang, K. Thornton, N.P. Dasgupta, Dendrites and pits: Untangling the complex behavior of lithium metal anodes through operando video microscopy. *ACS Cent. Sci.* 2 (2016) 790–801.

[43] K.H. Chen, K.N. Wood, E. Kazyak, W.S. LePage, A.L. Davis, A.J. Sanchez, N.P. Dasgupta, Dead lithium: Mass transport effects on voltage, capacity, and failure of lithium metal anodes. *J. Mater. Chem. A* 5 (2017) 11671–11681.

[44] G. Rong, X. Zhang, W. Zhao, Y. Qiu, M. Liu, F. Ye, Y. Xu, J. Chen, Y. Hou, W. Li, W. Duan, Y. Zhang, Liquid-phase electrochemical scanning electron microscopy for in situ investigation of lithium dendrite growth and dissolution. *Adv. Mater.* 29 (2017) 1606187.

[45] A. Pei, G.Y. Zheng, F.F. Shi, Y.Z. Li, Y. Cui, Nanoscale nucleation and growth of electrodeposited lithium metal. *Nano Lett.* 17 (2017) 1132–1139.

[46] H.J.S. SAND, III.On the concentration at the electrodes in a solution, with special reference to the liberation of hydrogen by electrolysis of a mixture of copper sulphate and sulphuric acid. *Philos. Mag.* 17 (1956) 496–534.

[47] J.N. Chazalviel, Electrochemical aspects of the generation of ramified metallic electrodeposits. *Phys. Rev. A* 42 (1990) 7355–7367.

[48] C. Yan, H. Yuan, H.S. Park, J.Q. Huang, Perspective on the critical role of interface for advanced batteries. *J. Energy Chem.* 47 (2020) 217–220.

[49] P. Shi, X.Q. Zhang, X. Shen, R. Zhang, H. Liu, Q. Zhang, A Review of Composite Lithium Metal Anode for Practical Applications. *Adv. Mater. Technol.* 5 (2020) 1900806.

Graphical abstract

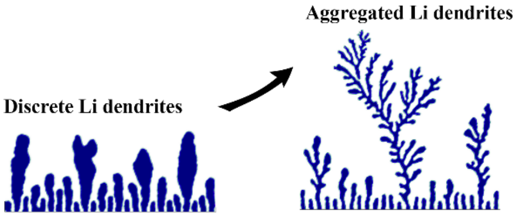

Multiscale imaging techniques in conjunction with phase field simulations reveals the morphological evolution and mechanistic understanding of aggregated Li dendrites.

Highlights

1) The transition of Li dendrites with increasing current densities is revealed.

2) In/ex-situ microscopy and phase field simulations are employed.

3) The locally concentrated electric field induces aggregated Li dendrites.

Declaration of interests

The authors declare no competing financial interests.